Elastic multiple scattering of surface plasmon polaritons: studies with a near-field optical microscope

V. Coello and J.M. Siqueiros
Centro de Ciencias de la Materia Condensada, Universidad Nacional Autónoma de México
Apartado postal 2681, 22800 Ensenada, Baja California, Mexico

Recibido el 25 de abril de 2000; aceptado el 6 de junio de 2000

Elastic (in the plane) scattering of surface plasmon polaritons is experimentally and theoretically investigated. Near-field optical images exhibited rather bright round spots that may be directly related to the phenomenon of strong SPP localization. Numerical simulations carried out have well reproduced the overall appearance of the observed hot spots. A calculated optical enhancement of several orders of magnitude larger than the average intensity field was found. An SPP microcomponent for two-dimensional SPP micro-optics was numerically carried out.

Keywords: Surface plasmon polaritons; near field optics

Se investiga el esparcimiento elástico de plasmones de superficie experimental y teóricamente. Las imágenes en el campo cercano exhibieron manchas redondas muy brillantes, las cuales podrían estar relacionadas directamente con el fenómeno de localización fuerte de plasmones de superficie. Simulaciones numéricas llevadas a cabo reprodujeron bien la apariencia general de las manchas brillantes observadas. Hemos calculado un ensanchamiento de varios órdenes de magnitud mayor que el promedio del campo de intensidad de los plasmones de superficie. Un microcomponente para una óptica bidimensional de plasmones de superficie fue numéricamente llevado a cabo.

Descriptores: Plasmones de superficie; óptica de campo cercano

PACS: 73.20.M; 61.16.C

1. Introduction

Surface plasmon polaritons (SPP) are oscillations of surface electron charge density, which can exist at a metal/dielectric interface [1]. Associated with them there exists an electromagnetic field propagating along the interface with exponential decays perpendicular to it. For this reason, SPP exhibit an extremely high sensitivity to surface properties such as roughness and surface adsorbates. Due to their electromagnetic nature, SPP are able to diffract, reflect, and interfere. These properties are clearly exhibited in the course of SPP scattering. Scattering of SPP is usually caused by randomly placed surface imperfections, since even the most carefully prepared surfaces are not completely flat. It should be stressed here that our main consideration is on the elastic SPP scattering in the surface plane and that SPP scattering into a free space is an unwanted process leading to the additional (radiative) losses experienced by the SPP.

For the last twenty years, in spite of the extensive investigation works on SPP [1], there exists not a complete understanding of elastic SPP scattering and related phenomena. This fact has been, at least partly, caused by the indirect (far-field) methods of detection of the SPP intensity field. However, a direct probe of SPP fields is not a simple task since evanescent fields do not carry away (in average) any energy. This impediment was successfully overcome with the birth of the scanning near-field optical microscopy (SNOM) techniques [2]. A photon scanning tunneling microscope (PSTM) [3], in which an uncoated fiber tip is used to detect an evanescent field of the light being totally internally reflected at the sample surface is apparently the most suitable technique for local probing of the SPP field, especially when combined with a shear force feedback system [4] for regulation of the tip-surface distance. Due to the relatively low refractive index of optical fibers, such a tip can be within certain approximations considered as a non-pertubative probe of the electric field intensity [5] and such a feedback system provides the possibility to measure the surface topography simultaneously with the near-field intensity distribution in the surface plane. The PSTM has been already used to measure the degree of SPP field enhancement [6] and the decay of the SPP evanescent field as a function of the tip-surface distance [7]. Recently, a work on direct observation of localized surface plasmon coupling using a PSTM was reported [8]. There, SPP were excited in gold nanostructures tailored by electron beam lithography. In this work, with the help of a PSTM we have studied the elastic scattering of SPP along metallic surfaces. Near-field optical images generated by SPP excited in different films were obtained simultaneously with their correspondent topography. We observed spatially localized enhancement of the SPP intensity field (strong localization) in a rough film. We have also carried out numerical simulations showing typical features of the regime of multiple scattering that may eventually result in strong SPP localization and compared them with experimental observations. Finally, a proposal for local controlling of SPP propagation was numerically demonstrated.

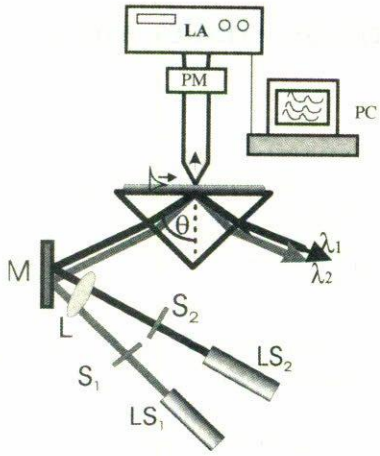

FIGURE 1. Illustration of the setup with the computer-controlled scanning near-field optical microscope. Two separate laser excitation sources, LS_1 and LS_2 are used in turn ($\lambda_1 = 633$ nm and $\lambda_2 = 544$ nm) by means of shutters controllers (S_1 and S_2). The laser beam is focused and directed by using a lens (L) and a plane mirror (M) through the SPP Krestchmann configuration. The optical signal is detected with a photomultiplier (PM) and a lock-in amplifier (LA) and processed using a personal computer (PC).

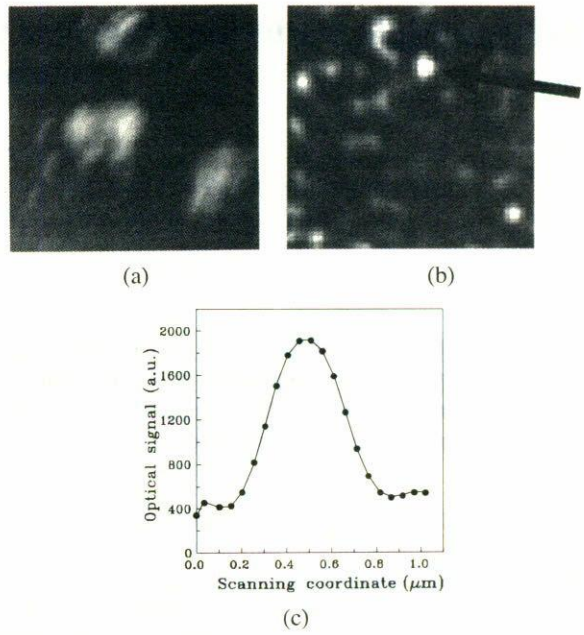

FIGURE 2. Gray scale (a) topographical and (b) near field optical image ($4 \times 4\,\mu m^2$) of individual randomly placed microscatterers on the gold film. (c) Cross section of the bright spot pointed out by the arrow in Fig. 3b. The maximum depth of the topographical image is 155 nm. Contrast of the near-field image is $\sim 98\%$.

2. Experimental arrangement

The experimental setup consists of a non-commercial PSTM combined with a shear-force feedback system and an arrangement for SPP excitation in the usual Kretschmann configuration (Fig. 1). The operational principle of the shear-force can be described in a general form as follows: a laterally vibrating optical fiber probe is illuminated (through the fiber and perpendicular to its axis) by a focused laser beam thus creating a time varying diffraction pattern where detection (with a photodiode) results in a signal proportional to the amplitude of the probe vibration. When the probe is brought near the surface, the amplitude of the probe vibration decreases, because of increased probe-sample interaction forces (shear forces). Thereby, the point when such amplitude becomes nearly zero is taken as the probe-sample contact point. The sample-tip distance is kept constant using a feedback system and we have estimated that such a distance is in a range of $\sim$ 10–15 nm [9]. The setup has been implemented for exciting SPP at either of two optical wavelengths *viz.* 633 and 544 nm. The scanning in our near-field microscope is carried out by means of a stand-alone scanner type, *i.e.*, the probe is scanned (using a piezotranslator) along a fixed sample, this fact allows one to keep the illumination configuration for SPP excitation without any change during scanning. The near-field optical probes used have been made from single mode silica fibers. The method of preparation consisted in $\sim$ 55 min etching of the optical fiber in 40% hydrofluoric acid. Concerning the detection of the optical signal, the SPP optical field is probed by the fiber tip and partially transmitted (in the form of propagating waves) through the fiber towards a photomultiplier tube. Finally, the signal is detected by means of a lock-in amplifier and processed using a personal computer. A typical value of the detected signal was observed in a range of 100–600 pW for red light, whereas for yellow light the range was of 5–200 pW. Typical acquisition time is ~ 30 min for a scan area of $\sim 4 \times 4\,\mu m^2$. The studied sample was a gold film thermally evaporated on the base of glass prism, which had previously been covered with a sublayer of colloidal gold particles (diameter $\sim$ 40 nm) dried up in atmosphere, therefore a surface roughness was randomly introduced along the sample surface. The thickness of the film was of ~ 58 nm.

3. Experimental results

First, a calibration of our PSTM was carried out in a similar way to that described elsewhere [9]. Near-field optical images taken near the surface (with shear force feedback) exhibited rather bright spots almost round in shape and with locations that are not correlated to the local surface profile (Figs. 2a and 2b). The size of the bright spots is of $\sim$ 300–400 nm and the maximum signal is up to 5 times larger than the background level (Fig. 2c). These features are similar to those previously observed with a rough gold film [10], and thereby can be related to the phenomenon of strong SPP localization caused by surface roughness. In another set of measurements (using the same film), SPP intensity distributions were mapped using, alternatively, both excitation wavelengths as it is shown in Fig. 3. The topographical image (Fig. 3a) showed a surface with randomly located gold particles (or particle clusters). The elongated appearance of the particles is probably

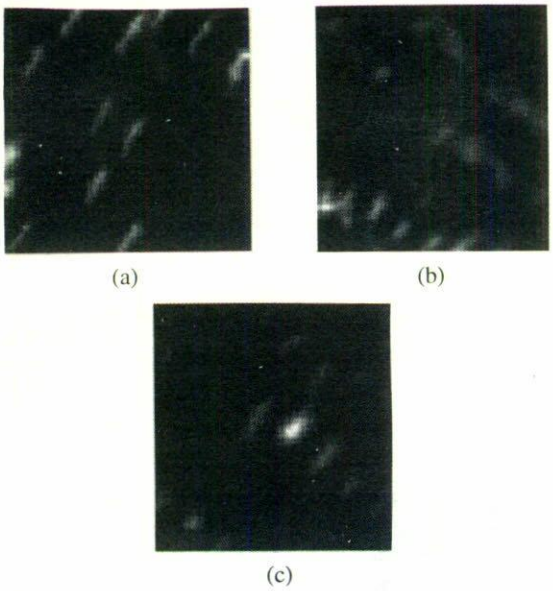

FIGURE 3. Gray scale (a) topographical and (b), (c) near field optical images ($4 \times 4\ \mu m^2$) of individual randomly placed microscatterers on a 53-nm-thick gold film. The optical images were recorded using in turn red (b) and yellow (c) excitation wavelengths. The depth of the topographical image is $\sim$ 42nm (a). Contrast of the optical images is $\sim$ 98% (b) and (c).

induced by an asymmetrical shape of the fiber tip (taking the relatively large cone-angle into account) and/or a tilt of the fiber axis with respect to the normal direction (to the film surface). The corresponding near-field optical images exhibited rather bright spots, that are almost round in shape and located differently for different wavelengths (Figs. 3b and 3c). This fact is completely justified since, in the regime of multiple scattering interference pattern are very sensitive to variations in wavelength, distribution of scatterers, phase distribution etc. It should be noted that, since the distribution of a colloid gold particle was not uniform, the film roughness and, consequently, the SPP scattering were found strongly varying across the sample. For example, the corresponding near-field optical images were often noticeably influenced by singular scattered waves (Fig. 3b and 3c). Actually, we believe that only the bright spots should be directly related to the excited and scattered SPP.

4. The model

From experimental work, it has been understood that the elastic SPP scattering can be considered to be approximately isotropic [11]. Therefore, simulations of SPP localization have been carried out by using the approximation of point-like dipolar scatterers [12]. Recently, we have proposed a model for modeling SPP multiple scattering on metallic surfaces [13]. In the model we have two main assumptions: (i) the elastic SPP scattering is dominant with respect to the inelastic one; (ii) the well-defined parabolic interference fringes observed with SPP scattering by individual defects correspond to the interference between the excited SPP with a plane phase front and the scattered SPP with a cylindrical phase front [11]. The two dimensional geometry of the elastic SPP scattering allows one to omit the exponential decays, perpendicular to the surface, inherent of the SPP field. That is to say, at any coordinate the total SPP field, $E(r)$ being a superposition of cylindrical SPP with the same wavenumber β (equal to that of a plane SPP) [14], exhibit the same spatial dependence along the direction perpendicular to the surface plane. Therefore, it is possible to write an expression for the total SPP field at an arbitrary point r (which does not coincide with the position of any scatterer) as follows:

$$E(\mathbf{r}) = E_0(\mathbf{r}) + \sum_{j=1}^{N} \alpha_j E(\mathbf{r}_j) G(\mathbf{r}, \mathbf{r}_j), \qquad (1)$$

with

$$G(\mathbf{r}, \mathbf{r}_j) = \frac{i}{4} H_0^{(1)}(\beta |\mathbf{r} - \mathbf{r}_j|),$$

where E_0 is the incident SPP field, α_j is the effective (dimensionless) polarizability of the jth scatterer located at the surface coordinate $\mathbf{r}_j$ and it corresponds to the scatterer's strength (as far as the elastic SPP scattering is concerned), N is the number of scatterers, H is the Hankel function and β is the SPP propagation constant. Eq. (1) is a self-consistent equation of multiple scattering, and in order to solve it, the polarizabilitie, α, as well as the self-consistent field at the sites of the scatterers $E(r_j)$ has to be calculated. The polarizability calculation, usually rather complicated [15], can be circumvented by the use of the recorded near-field optical images, *i.e.*, by fitting α such that experimental and calculated images would have the same optical contrast. Concerning the self-consistent field, $E(r_j)$, if the regime of multiple SPP scattering prevails, the successive Born iterations, n, should be used to calculate it, thus

$$E^n(\mathbf{r}_j) = E_0(\mathbf{r}_l) + \sum_{l=1, l\neq 1}^{N} \alpha_j E^{n-1}(\mathbf{r}_l) G(\mathbf{r}_j, \mathbf{r}_l). \qquad (2)$$

If the resonance iteration is rather strong, as it could be in the case of SPP localization [10], the Born iterations became divergent and the exact solution of the self-consistent Eq. (1) has to be employed. In our case we observe that only a few iterations ($n < 10$) were sufficient to obtain stable values of the self-consistent field at the site of the scatterer.

5. Numerical simulations

We have performed numerical simulations for a total area of $3 \times 3\,\mu m^2$ where 40 scatterers randomly distributed (with $\alpha = 3$) are illuminated by a plane wave propagating from left to right. The SPP propagation length [1], $L = 27\,\mu m$, is noticeable larger than the dimension of total calculated area as in the case of the experiments where we observed a value of $L \sim 15\,\mu m$ in an area of $5 \times 5\,\mu m^2$. We obtained round bright spots for the calculated intensity distributions (Fig. 4a) with an overall appearance quite similar to those experimen-

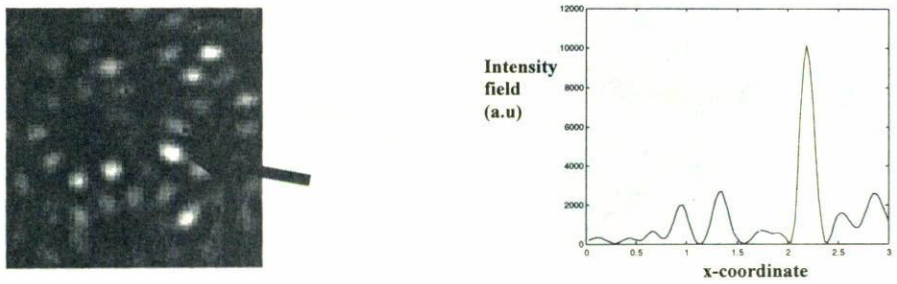

(a) (b)

FIGURE 4. Gray Scale representation (a) of the total field intensity distribution in the area of $5 \times 5\ \mu m^2$ calculated in the regime of multiple scattering (by 40 scatterers with $\alpha = 3$ randomly distributed in the area) for red wavelength. (b) Cross section of the calculated intensity distribution for the bright spots pointed out by the arrow.

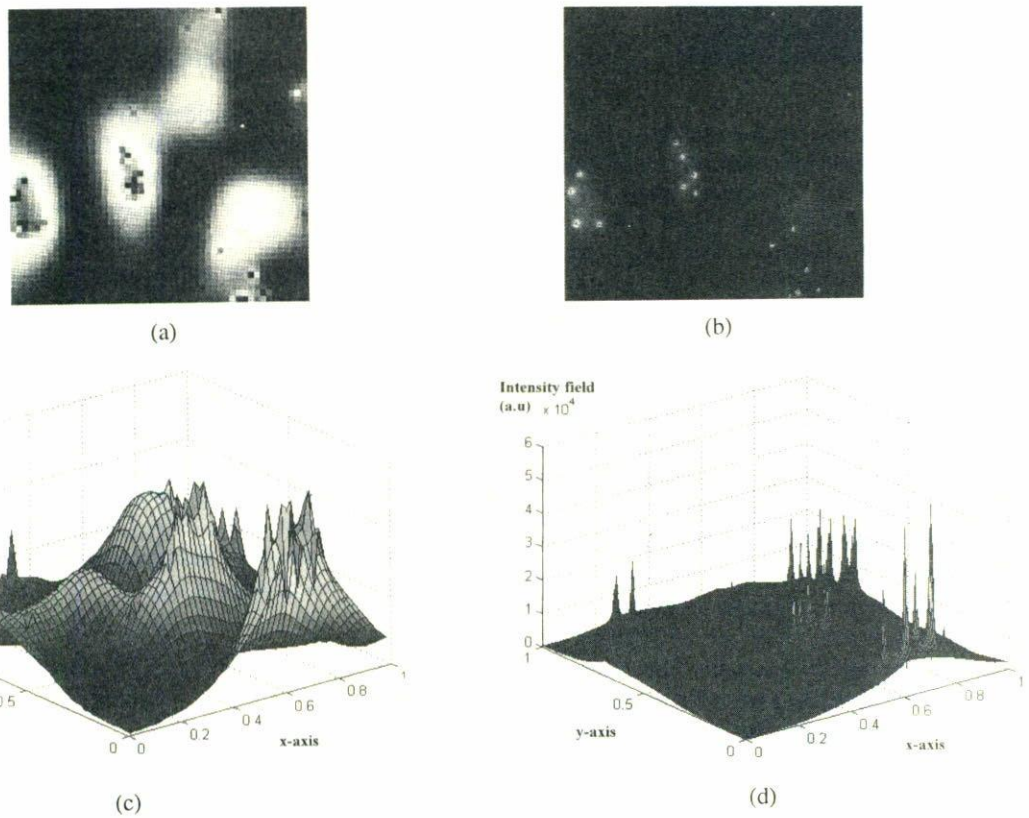

(a) (b)

(c) (d)

FIGURE 5. Gray scale representation of the total field intensity distributions calculated in an area of $1 \times 1\ \mu m^2$ using (a) 100×100 and (b) 200×200 points and for red wavelength. Three-dimensional perspective of the total intensity field distribution of (c) Fig. 5a and (d) Fig. 5b.

tally observed (Figs. 2b, 2c, and 3b). The calculated enhancement of the intensity field was clearly shown by taking the corresponding cross section of a resultant bright spot (Fig. 4b), where a maximum intensity value of 10^4 times larger than the average intensity level was exhibited.

SPP localization is difficult to achieve and even for rough gold films is not automatic. In general it is not easy to find media in which one can get short mean free paths. For instances, it is not convenient to make the volume fraction of scatterers larger and larger since it would lead not only to elastic but also to inelastic SPP scattering which may cause the optical signal to be dominated by propagating components [9]. However one of the reasons for the absence of bright spots in the experiments is the technically limited resolution of the microscope. Very small bright spots stand out from larger spots with lower intensities. Taking this fact into account, we have developed numerical simulations of elastic multiple scattering of SPP in an area of $1 \times 1\ \mu m^2$ formed by 100×100 calculated points (Figs. 5a and 5c) and then increased the number of calculated point, *i.e.*, the resolution, up to 200×200 keeping exactly the same numerical conditions (Figs. 5b and 5d). It is clear from a comparison between

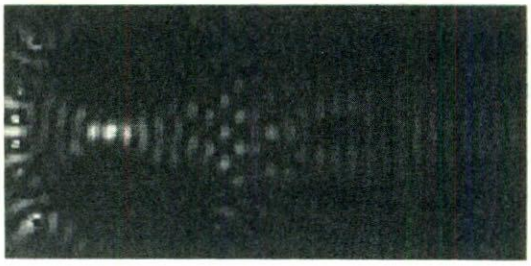

FIGURE 6. Gray-scale representation of the total field intensity distribution of two parabolic mircromirrors facing each other (resonator) for red light. The intensity distribution was calculated within an area of $10 \times 5\,\mu m^2$. Contrast of the image is 100%.

Figs. 5a and 5c and Figs. 5b and 5d that details in the SPP intensity fields (*e.g.* sharp peaks) that are somewhat shadowed in simulations obtained with a poor resolution (Figs. 5a and 5c) can be clearly seen when using a higher resolution (Figs. 5b and 5d). In Fig. 5b, we can observe very small bright spots emerging from larger spots (Fig. 5a) and with an enhancement of the intensity field up to 5×10^4 times with respect to the average field value (Fig. 5d).

Finally, we show results on an important point related to the SPP phenomena: the local control of the SPP propagation. Based on a successfully proved idea about a two dimensional micro-optics of SPP [11], we developed a numerical simulation (for red light) of two curved 16-scatterer micromirrors facing each other forming a nearly concentric optical cavity, which is able to carry out SPP optical enhancement in a controlled form (Fig. 6). Ideally, a focusing micromirror should consist of scatterers placed along a parabolic curve $y^2 = 4Fx$ where (x, y) is the orthogonal coordinate system in the surface plane. The x-axis is oriented along the optical axis and F is the focal length. The two simulated 16-scatterer micromirrors with $F = 2\mu m$ exhibited good stability and large focusing effect along the optical axis (Fig. 6). In the simulated cavity, $F_1 \leq d/2$; $F_2 \leq d/2$ for the left and the right mirror, respectively, being $d_{1,2} = 4.5\,\mu m$ the cavity length. Nevertheless, such a cavity showed that complicated SPP microstructures exhibit rather strong wavelength dispersion and configurational instability (*i.e.*, instability with respect to geometrical variations) in the overall scattering behavior. Several factors have to be further elucidated for this kind of microcavities to obtain stable behavior, for example, the adequate values of the polarizability of the individual microscatterers, which will depend on the particular experimental conditions.

6. Conclusions

Elastic SPP scattering by randomly distributed scatterers has been, experimentally and theoretically investigated. We recorded near-field optical images with electromagnetic localized modes in the form of round bright spots with an enhancement ratio up to 5 times larger than the background signal. As far as calculations are concerned, relatively straightforward simulations were obtained. We believe that our numerical simulations can be used to clarify many features associated to the SPP localization and that they will be greatly improved as more experimental data become available. Thus, a certain understanding of some of the features inherent to the subwavelength light interference phenomena was gained but it is clear from the outcome of this study that more systematic work in this context is still needed. We suggest a different approach for future work, such a statistical studies [16].

Acknowledgments

We thank M. Sc. Carlos Gonzales for his helpful computational assistance.

1. H. Raether, "Surface Plasmons",*Springer Tracts in Modern Physics* **111**, (Springer, Berlin, 1988); *Surface Polaritons*, edited by V.M. Agranovich and D.L. Mills, (North-Holland, Amsterdam, 1982).
2. *Near Field Optics*, edited by D.W. Pohl and D. Courjon, (Kluwer, The Netherlands, 1993); D. Courjon and C. Bainier, *Rep. Prog. Phys.* **57** (1994) 989.
3. R.C. Reddick, R.J. Warmack, and T.L. Ferrel, *Phys. Rev. B* **39** (1989) 767; D. Courjon, K. Sarayeddine, and M. Spajer, *Opt. Commun.* **71** (1989) 23; F. de Fornel *et al.*, *Proc. SPIE* **1139** (1989) 77.
4. A. Schchemelin *et al.*, *Rev. Sci. Instrum.* **64** (1993) 3528.
5. J.J. Greffet and R. Carminati, *Prog, Surf, Sci.* **56** (1997) 133.
6. P.M. Adam, L. Salomon, F. de Fornel, and J.P. Goudonnet, *Phys. Rev. B* **48** (1993) 2680.
7. H. Bielefeldt *et al.*, *Near Field Optics*, edited by D.W. Pohl and D. Courjon, (Kluwer, The Netherlands, 1993) p. 281.
8. J.R. Krenn *et al*, *Phys. Rev. Lett* **82** (1999) 2590; Jean-Claude Weeber *et al*, *Phys. Rev. B* **60** (1999) 9061.
9. V. Coello, S.I. Bozhevolnyi, and F.A. Pudonin, *Proc. SPIE* **3098** (1997) 536.
10. S.I. Bozhevolnyi, *Phys. Rev. B* **54** (1996) 8177.
11. I.I. Smolyaninov, D.L. Mazzoni, and C.C. Davis, *Phys. Rev. Lett.* **77** (1996) 3877; S.I. Bozhevolnyi and F.A. Pudonin, *Phys. Rev. Lett.* **78** (1997) 2823.
12. L. Novotny, B. Hecht, and D.W. Pohl, *J. Appl. Phys.* **81** (1997) 1798.
13. S.I. Bozvevolnyi and Victor Coello, *Phys. Rev. B* **58** (1998) 10899.
14. V.A. Kosobukin, *Phys. Solid State* **35** (1993) 457; P.J. Valle, E.M. Ortiz, and J.M. Saiz, *Opt. Commun.* **137** (1997) 334.
15. A.V. Shchegrov, I.V. Novikov, and A.A. Maradudin, *Phys. Rev. Lett.* **78** (1997) 4269.
16. M. Stockman, *Phys. Rev. Lett.* **72** (1994) 2486.